Journal of Materials Chemistry B

ROYAL SOCIETY OF CHEMISTRY

PAPER

View Article Online
View Journal | View Issue

Cite this: J. Mater. Chem. B, 2025, 13, 1690

Quercetin nanocrystal-loaded alginate hydrogel patch for wound healing applications†

Malay Nayak,‡ Vivek Kumar,‡ Durba Banerjee, Lipi Pradhan, Prajwal Kamath and Sudip Mukherjee *

Received 31st July 2024,
Accepted 11th December 2024

DOI: 10.1039/d4tb01699h

rsc.li/materials-b

Wound healing can often be delayed due to non-favourable physiological conditions. Current treatment strategies have many limitations, and the development of novel therapeutic patches is urgently required. Herein, we have developed a hydrogel-based wound healing patch containing quercetin nanocrystals to enhance quercetin solubility, leading to sustained release and improved bioactivity. Due to the antioxidant properties of quercetin, a sustained release of the drug is highly beneficial for the rapid repair of wounds by reducing oxidative stress. Quercetin nanocrystals with a size of 600–800 nm were synthesized that demonstrated sustained release of quercetin when fabricated in a hydrogel patch. This has been utilized for *in vivo* wound repair in rat and mouse models of skin wounds. Overall, our study demonstrates the usability of a novel therapeutic hydrogel patch containing phytochemical-based nanocrystals for rapid wound healing applications.

1. Introduction

The human body possesses a remarkable ability to naturally heal itself after injury. When the skin, our body's largest organ, is breached, a complex biological cascade known as wound healing kicks in.[1] This intricate process, orchestrated by various cell types and signalling molecules, can be broadly divided into distinct phases: inflammation, proliferation, and remodelling.[2,3] During the inflammatory phase, the body aims to stem blood loss, prevent infection, and clear away damaged tissue. This is followed by the proliferative phase, where new blood vessels are formed (angiogenesis), and fibroblasts deposit collagen, the main structural protein of the skin.[2,4] Finally, the remodelling phase involves the reorganization and strengthening of the newly formed tissue to restore its original functionality.[2] However, wounds often experience disruptions in this process, leading to delayed healing, increased risk of infection, and significant discomfort. This necessitates wound healing therapies that can promote efficient, faster closure, reduce inflammation, and create a favourable environment for tissue regeneration.

Quercetin, a naturally occurring flavonoid found in fruits and vegetables, has emerged as a promising candidate due to its multifaceted therapeutic properties.[5] It boasts potent antioxidant activity, meaning it can neutralize harmful free radicals that contribute to tissue damage and inflammation.[6] Additionally, quercetin exhibits anti-inflammatory[7] and antimicrobial effects,[8] further promoting a favourable wound-healing environment. Despite its therapeutic potential, quercetin suffers from poor aqueous solubility and bioavailability, limiting its effectiveness when administered conventionally.[9] Existing research has explored quercetin's wound healing potential through various pathways, including Wnt/β-catenin signalling,[10] integrin expression changes,[11] and modulation of cytokine/growth factor activity.[12]

Nanocrystals, nanoparticles typically ranging from 1–100 nm in size, offer exciting possibilities for drug delivery.[13] By converting quercetin into nanocrystals, we can significantly improve its aqueous solubility and bioavailability, ultimately leading to enhanced therapeutic efficacy.[14] Hydrogels, three-dimensional networks capable of holding large amounts of water, have revolutionized drug delivery systems for wound healing applications.[15] Their biocompatibility and ability to create a moist environment that promotes cell migration makes them candidates for wound dressings. Among various hydrogels, alginate hydrogels derived from seaweed stand out due to their excellent biocompatibility, inherent wound-healing properties, and ability to gel readily in the presence of calcium ions, simplifying their application.[16–18]

In this study, we reported the successful fabrication of a quercetin nanocrystal-loaded alginate hydrogel patch (Scheme 1). This patch exhibited sustained release properties, allowing for a continuous supply of quercetin to the wound site. Moreover, the patch demonstrated significant antioxidant activity, potentially mitigating tissue damage and promoting healing. *In vitro* and

School of Biomedical Engineering, IIT (BHU), Varanasi, 221005, UP, India.
E-mail: sudip.bme@iitbhu.ac.in; Tel: +91-7980659213

† Electronic supplementary information (ESI) available. See DOI: https://doi.org/10.1039/d4tb01699h

‡ Equally contributing first authors.

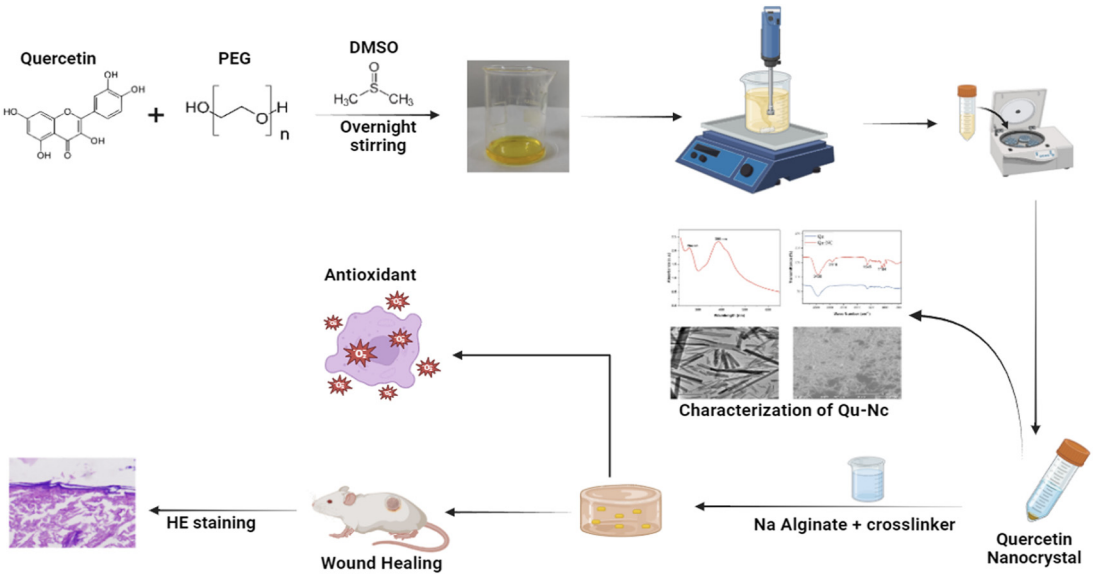

Scheme 1 Graphical abstract of synthesis, characterization and biomedical application of Qu–NCs as an antioxidant and wound healing agent.

in vivo studies confirmed the superior wound healing efficacy of this patch compared to control and blank hydrogel groups.

2. Materials and methods

2.1 Materials

Quercetin, high viscous sodium alginate, low viscous sodium alginate, barium chloride, DPPH (2,2-diphenyl-1-picrylhydrazyl), PBS, DMSO, PEG 400, ethanol, 5,5′-dithiobis-(2-nitrobenzoic acid) (DTNB), Bradford reagent, trichloroacetic acid, Triton X-100, streptozotocin and 3-(4,5-dimethylthiazol-2-yl)-2,5-diphenyltetrazolium bromide (MTT) were obtained from SRL (Sisco Research Laboratories Pvt. Ltd) – India. DMEM cell culture media and Fetal bovine serum (FBS) were ordered from HiMedia Laboratories Pvt. Ltd. Primary antibody CD163 monoclonal antibody (14-1631-82) and alpha smooth muscle actin monoclonal antibody (1A4) were purchased from eBioscience™ (cat no: 14-9760-82). Goat anti-mouse IgG2a secondary antibody, Alexa FluorTM 594 (cat no: A21135), and collagen 1 polyclonal antibody (cat no: BS-10423R) were purchased from Invitrogen.

2.2 Preparation of quercetin nanocrystals

Quercetin nanocrystals were prepared by the following process. Initially, 8.0 mg of quercetin was dissolved in 1 mL DMSO. 1 g PEG was then added, and the mixture was stirred overnight at 40 °C. The mixture was subsequently added dropwise to 50 mL of 4 °C Milli-Q water under magnetic stirring, followed by homogenization for 1 hour to form the nanocrystals. The resulting suspension was then centrifuged (50 minutes, 3000 rpm, 4 °C) to separate the nanocrystals. The supernatant was discarded, and the combined pellets were re-suspended in 25 mL of 4 °C Milli-Q water. This re-suspended solution was again centrifuged (50 minutes, 3000 rpm, 4 °C) to remove any residual impurities. The final pellet, containing the quercetin nanocrystals (Qu–NC), was collected after discarding the supernatant, and the pellet was collected for future use. The concentration of the pellet was 5.7 mg mL^{-1}.

2.3 Preparation of a Na alginate hydrogel patch with quercetin

High viscosity (HV) and low viscosity (LV) sodium alginate stock solutions (3% w/v) were prepared by dissolving the respective alginates in Milli-Q water at 80 °C with vigorous stirring. To create the Qu–NC loaded hydrogel patch, 60 μL of high viscosity alginate, 90 μL of low viscosity alginate and 15 μL of Qu–NC solution (concentration of 5.7 mg mL^{-1}) were mixed thoroughly and poured into an 8 mm diameter hydrogel patch. Subsequently, a crosslinking solution containing 0.6% barium chloride was sprayed evenly at the bottom of the mold as well as all above the alginate solution. The mold was gelated overnight at 40 °C to get the final hydrogel patch.

2.4 Characterisation of Qu–NCs

2.4.1 UV visible spectroscopy. The UV-visible absorption spectra of both quercetin (Qu) and the quercetin nanocrystals (Qu–NCs) were measured at a concentration of 1 mg mL^{-1} using an Eppendorf UVette machine. The scan range covered wavelengths from 200 to 800 nm.

2.4.2 TEM. The morphology of the synthesized quercetin nanocrystals (Qu–NCs) was investigated using transmission electron microscopy (TEM) performed on a Tecnai G2 20 TWIN instrument. A dilute Qu–NC suspension was prepared, and a few drops were deposited onto copper TEM grids coated with a carbon film. After allowing the sample to settle overnight, the grids were loaded into the TEM operated at an acceleration voltage of 200 kV for imaging. The SAED pattern of the Qu–NCs was also analysed using the same instrument.

2.4.3 SEM. The size and shape of the synthesized quercetin nanocrystals (Qu–NCs) were characterized using scanning electron microscopy (SEM) performed on a JEOL JSM instrument operating at 20 kV. A few drops of the diluted solution were then cast onto a coverslip and allowed to air-dry at 37 °C overnight. Subsequently, the sample was scanned in the SEM, and photomicrographs were captured.

2.4.4 FTIR. The functional groups of quercetin and the biosynthesized quercetin nanocrystals (Qu–NCs) were investigated using Fourier-transform infrared (FT-IR) spectroscopy. One milligram each of lyophilized quercetin and Qu–NCs were combined with FT-IR grade KBr and compressed into discs using a hydraulic press. A Nicolet iS5 FT-IR spectrophotometer was employed to analyze the discs across a wavenumber range of 400–4000 cm^{-1}.

2.5 NC release study

To determine the concentration of quercetin nanocrystals (Qu–NCs), a calibration curve was constructed. A series of Qu–NC solutions were prepared in ethanol at varying concentrations: 100, 75, 50, 25, 10, 1, and 0.1 μg mL^{-1}. The absorbance of each solution was measured at 380 nm using a UV spectrophotometer with 100% concentrated ethanol as the reference. Subsequently, using Origin software, the absorbance values were plotted against their corresponding concentrations. A linear regression analysis was performed to obtain a calibration curve with a zero-intercept, allowing for the calculation of unknown Qu–NC concentrations based on their absorbance at 380 nm.

The *in vitro* release kinetics of quercetin from the Qu–NC hydrogel patch were investigated over 18 days. A freshly prepared patch was placed in a 24-well plate containing 2 mL of phosphate-buffered saline (PBS) (day 0). At predetermined time points (1, 2, 3, 4, 5, 6, 12, and 18 days), 1 mL of the release medium (PBS) was collected and replaced with fresh PBS. The collected PBS samples were analyzed using UV-visible spectroscopy (Eppendorf UVette) at 380 nm to quantify quercetin release. The absorbance measurements were compared to a PBS blank as a control. This method allowed for the monitoring of quercetin release from the Qu–NC hydrogel over the course of the experiment.

2.6 Degradation study of the hydrogel

To evaluate the degradation behaviour of the hydrogels, preweighed samples ($n = 3$) with a diameter of 8 mm (both Qu–NC loaded and blank) were immersed in phosphate-buffered saline (PBS) at 37 °C. At predetermined time points (days 0, 3, 5, 7, and 12), the hydrogels were retrieved from the PBS solution and weighed again. The weight change over time was quantified by calculating the weight percentage (% weight) using the following equation:

$$\%\ \text{weight} = (\text{final weight at time point } t/\text{initial weight at day 0}) \times 100.$$

Additionally, the morphology of the hydrogels at each time point was captured using microscopy to assess any visual changes associated with degradation.

2.7 Compressive test of Qu–NC hydrogel

The mechanical properties of the quercetin nanocrystal (Qu–NC) loaded hydrogel and the blank alginate hydrogel were evaluated using a compression test. Cylindrical samples of both hydrogels with identical dimensions (8 mm diameter and 3.5 mm height) were subjected to controlled compression using a Brookfield TexturePro CT instrument. The hydrogels were placed on the test platform under standardized conditions (0.07 N trigger load, 0.50 mm s^{-1} test/return speed, TA42 probe). The compression test involved applying a 15% and 10% strain (compression) to the hydrogels. Triplicate measurements were performed for each hydrogel type to ensure data reliability.[19]

2.8 Chick embryo chorioallantoic membrane (CAM) assay

To assess the biocompatibility and potential for angiogenesis of the quercetin nanocrystal (Qu–NC) loaded hydrogel, the chorioallantoic membrane (CAM) assay was performed in triplicate.[20] Fertilized chicken eggs were incubated at 37 °C for four days. After creating a window in the eggshell to access the CAM, 10 mm diameter samples of Qu–NC hydrogel, blank hydrogel, and control were applied to the CAM. The CAM development and blood vessel formation were monitored at baseline and after eight and twelve hours of incubation using a Magnus MagZoom TZM6 Trinocular Stereo Zoom Microscope. This process allowed for the subsequent quantification of vessel area, junction number, and total vessel length to evaluate the effects of the hydrogels on blood vessel morphology.

2.9 Radical scavenging and *in vitro* ROS clearance assay

The free radical scavenging potential of the quercetin nanocrystal (Qu–NC) complex, Qu–NC hydrogel, and free quercetin were evaluated using a previously established DPPH (2,2-diphenyl-1-picrylhydrazyl) radical scavenging assay.[21] Varying concentrations (10, 25, 50, 84, and 100 μmol) of each sample were prepared in ethanol and added to a freshly prepared DPPH solution (60 μmol in methanol). After 25 minutes of incubation, the reduction in DPPH free radicals was measured by absorbance at 517 nm. A blank solution containing only DPPH served as the control. The percentage of radical scavenging activity (RSA%) was calculated for all samples using the equation:

$$\text{RSA\%} = 100 \times (\text{AC} - \text{AS})/\text{AC},$$

where AC and AS represent the absorbance of the control and sample solutions, respectively.

To check the ROS clearance from bacteria, the experiment involved monitoring the oxidation of 7′-dichlorodihydrofluorescein diacetate (DCFDA) to green fluorescent dichlorofluorescein (DCF) by intracellular reactive oxygen species (ROS). DCF produces green fluorescent light when it is oxidized by ROS. The bacterial suspensions (200 μL) were placed onto a 24-well plate and then treated with the Qu–NC hydrogel patch, followed by an incubation at 37 °C for 12 hours. After that, they were treated with 50 μL of 10 mM of H2 DCFDA in a black 96-well plate for 5 minutes at 25 °C. The green fluorescence

intensity was measured after 5 minutes using the excitation wavelength of 485 nm and emission wavelength of 528 nm.

2.10 *In vivo* wound healing studies in rats

The *in vivo* wound healing efficacy of the quercetin nanocrystal (Qu–NC) loaded hydrogel was evaluated in a full-thickness excision model on the dorsal side of Wistar rats. Healthy Wistar rats (6–7 weeks old; 200–300 g) were procured from the CDRI-Lucknow and maintained as per biosafety standards. Following institutional ethical approval (IIT(BHU)/IAEC/2023/068; approval date: February 9, 2023), healthy rats (6–7 weeks old, 200–300 g) were acclimatized for 7 days. Circular wounds with a standardized diameter of 10 mm were created using a biopsy punch. The rats were then divided into three groups: Qu–NC hydrogel (delivering 84 μg quercetin per patch), blank hydrogel, and a control with no treatment (each group contains 3 rats). All groups received topical application of their respective treatments on days 0, 3, 7, and 10. The hydrogels were secured with adhesive tapes, and wound closure was monitored and measured through digital imaging at designated time points (days 0, 3, 7, and 10).

2.11 Histology and immunohistochemistry:

Skin tissue samples were embedded in an optimal cutting temperature (OCT) compound and sectioned into 20 μm thick slices using a cryo-microtome. Sections were mounted on glass slides and rehydrated through a graded ethanol series (100%, 90%, 70%, 50%) followed by a PBS wash. Hematoxylin and eosin staining were done by using the published protocol.[22] For collagen staining, subsequently, slides were stained with 0.5% aniline blue solution for 5 minutes, rinsed in running tap water, and dehydrated through a graded ethanol series prior to mounting and visualization under a light microscope. For the immunohistochemistry of α-SMA, CD163 and collagen, the tissue slide rehydration was performed through a graded ethanol series (100%, 90%, 70%, 50%) followed by a PBS wash. Antigen retrieval was achieved by incubating sections in citrate buffer at boiling temperature for 5 minutes. After cooling and subsequent PBS washing, the sections were permeabilized with 0.5% Triton X-100 and blocked with 6% BSA and 0.3% Triton X-100 in PBS for 1 hour. Primary antibody was applied overnight at 4 °C, followed by multiple PBS washes. The secondary antibody diluted in blocking solution was incubated for 1 hour, and sections were again washed with PBS before imaging under a confocal microscope.

2.12 *In vivo* wound healing in diabetic mice

Following institutional ethical approval (IIT(BHU)/IAEC/2023/068; approval date: February 9, 2023), healthy mice (8–12 weeks old, 15–25 g) were acclimatized for 7 days. An *in vivo*, ROS model was generated by injecting streptozotocin (50 mg kg^{-1} in cold citrate buffer) intraperitoneally into the BALB/c mice two days before wound creation. After two days, the blood glucose level was monitored to confirm blood glucose over 250 mg dL^{-1} and a dorsal wound was created (6 mm diameter). The mice were then divided into three groups: Qu–NC hydrogel (delivering 84 μg quercetin per patch), blank hydrogel, and an untreated control with no treatment (n = 3). All groups received topical application of their respective treatments on days 1, 3, 5, and 7. The hydrogels were secured with adhesive tape, and wound closure was monitored and measured through digital imaging at designated time points (days 1, 3, 5, 7 and 9).[23]

2.13 *In vivo* antioxidant property evaluation

The wound tissues were collected and washed with PBS and then mixed with RIPA buffer for 30 min. After that, the tissue mixture was homogenised and then centrifuged to get the supernatant for further assays.

2.13.1 Protein quantification (Bradford assay). Protein concentrations in the tissue homogenates were determined using the Bradford assay. Briefly, protein samples were mixed with Bradford reagent, which binds to proteins and forms a colored complex. The absorbance of the complex was measured at 595 nm, and protein concentrations were calculated using a standard curve.

2.13.2 Reduced glutathione (GSH) assay. GSH levels were determined using Ellman's reagent. Tissue homogenates were mixed with trichloroacetic acid (TCA) to precipitate proteins. The supernatant was then reacted with Ellman's reagent, resulting in a colorimetric change that was measured at 412 nm. GSH concentrations were calculated by comparing the absorbance values to a standard curve.

2.13.3 Lipid peroxidation assay (TBARS). Lipid peroxidation, an indicator of oxidative stress, was assessed using the thiobarbituric acid reactive substances (TBARS) assay. Tissue homogenates were incubated with thiobarbituric acid (TBA) at high temperature, resulting in the formation of a pink-colored complex. The absorbance of this complex was measured at 532 nm, and TBARS levels were calculated using a standard curve.

2.14 Statistical analysis

Three independent experimental investigations were conducted to ensure this study's correctness and consistency. The mean value and standard error were used to illustrate the outcomes for every experiment. One-way analysis of variance (ANOVA) was utilized in the statistical study performed using Origin software to determine if the observed data had any relevance.

3. Results and discussion

The present study focused on fabricating a quercetin nanocrystal (Qu–NC) incorporated alginate hydrogel patch with antioxidant properties for rapid wound healing applications. Qu–NC and hydrogel patches were systematically characterized using different physiochemical techniques, and the *in vitro* and *in vivo* experiments were carried out (Scheme 1).

3.1 Qu–NC preparation and analysis validate the stability and production of the nanoparticle

Quercetin nanocrystals were prepared by a bottom-up method by using PEG-400 as a stabilizer. The Qu–NC pellet was yellowish in

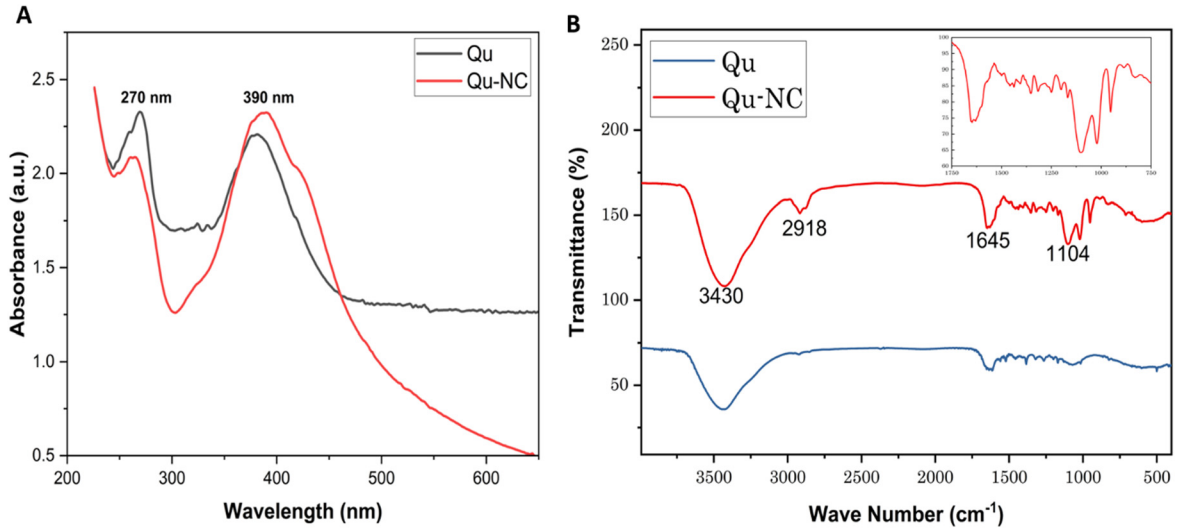

Fig. 1 Characterisation of Qu–NCs: (A) UV absorbance spectrum of Qu–NCs; (B) FT-IR spectrum of Qu–NCs and quercetin.

colour and found to be immiscible in water but soluble in the organic solvent. The formation of Qu–NC was confirmed by UV-visible spectroscopy. Qu–NC shows a clear peak at 264–270 and 386–390 nm, as shown in Fig. 1A, which confirms the formation of the quercetin nanocrystal[24] (Fig. 1B). Fourier-transform infrared spectroscopy (FT-IR) analysis was employed to characterize the functional groups present in both Qu–NC and quercetin drug. The technique probes the vibrational modes of molecules, providing information about their chemical functionalities.[25] As depicted in Fig. 1B, the FT-IR spectra of Qu–NC and quercetin exhibit distinct peaks. The Qu–NC spectrum reveals prominent absorption bands at 3430 cm^{-1}, 2918 cm^{-1}, 1645 cm^{-1}, and 1104 cm^{-1}. The bands at 3430 cm^{-1} and 2918 cm^{-1} are characteristic of O–H stretching vibrations, potentially indicative of hydroxyl groups (alcohols). The peaks at 1645 cm^{-1} and 1104 cm^{-1} can be attributed to C=C and C–O stretching vibrations, respectively, suggesting the presence of aromatic rings and ether or ester linkages.[26] The FTIR results confirm the presence of quercetin in Qu–NC.

Transmission electron microscopy (TEM) analysis was employed to investigate the morphology and size distribution of the synthesized Qu–NCs (Fig. 2A and B). The TEM images revealed a predominantly rod-shaped morphology with uniform distribution throughout the sample. The average size of the Qu–NCs, determined by image analysis, was 609 ± 196 nm. The scanning electron microscopy (SEM) results also confirmed the rod-shaped structure of the nanocrystals with uniform size (Fig. 2D). To elucidate the solid-state crystalline structure of the Qu–NCs, selected area electron diffraction (SAED) analysis was performed. The SAED pattern (Fig. 2C) displayed distinct diffraction rings corresponding to specific interplanar distances within the crystalline lattice.[27] Based on the SAED pattern analysis, the intermolecular distances within the Qu–NC crystals were calculated to be 3.4695 Å, 7.3273 Å, and 1.7210 Å. These interplanar spacings can be further utilized for crystal structure identification using reference databases. Moreover, by converting the quercetin drug to a nanocrystal, the solubility of the drug is increased (Fig. S2, ESI†). To check the increased bioavailability, a known amount (1 mg mL^{-1}) of bulk quercetin and Qu–NC was dispersed in PBS and assayed with sedimentation kinetics at 0, 30, and 60 minutes. It has been observed that the sedimentation rate of Qu–NC was significantly slow, indicating excellent solubility compared to bulk quercetin, which is poorly soluble in aqueous media. It is evident that at 1 h, bulk quercetin settled down completely, whereas, in the case of Qu–NC, the settling rate was low (Fig. S2, ESI†). Increased dispersibility has been reported to be linked with the enhanced bioavailability of the compound.[28]

3.2 Qu–NC loaded hydrogel patches show slow and sustained release of drugs

The fabricated quercetin nanocrystal (Qu–NC) loaded alginate hydrogel patch exhibited a well-defined circular shape with a diameter of 8 mm and a thickness of 2 mm (Fig. 3A).

Notably, the blank hydrogel displayed a whitish-ash colour, whereas the Qu–NC loaded hydrogel appeared brownish-yellow (Fig. 3B). This colour difference is likely due to the incorporation of quercetin nanocrystals within the hydrogel matrix. Drug loading optimization was done by taking various volumes of Qu–NC solution (5, 10, 15, 20, and 25 μL) within the hydrogel. The corresponding drug amount to each hydrogel came as 28, 56, 84, 112 and 140 μg; respectively. Hydrogels formulated with 20 and 25 μL of Qu–NC exhibited excessive swelling, likely due to disruptions in the hydrogel crosslinking structure (Fig. S5, ESI†). Considering the stability and suitability for wound healing applications, a Qu–NC volume of 15 μL was selected for hydrogel fabrication with a maximum drug loading efficiency. The *in vitro* release profile of quercetin from the Qu–NC hydrogel patch was investigated using UV-visible spectroscopy (Fig. 3C and D). The release study demonstrated a sustained and controlled release of quercetin from the hydrogel patch over an 18-day period (Fig. 3D). By day 18, 96.86% of the encapsulated quercetin was released from the patch. The release

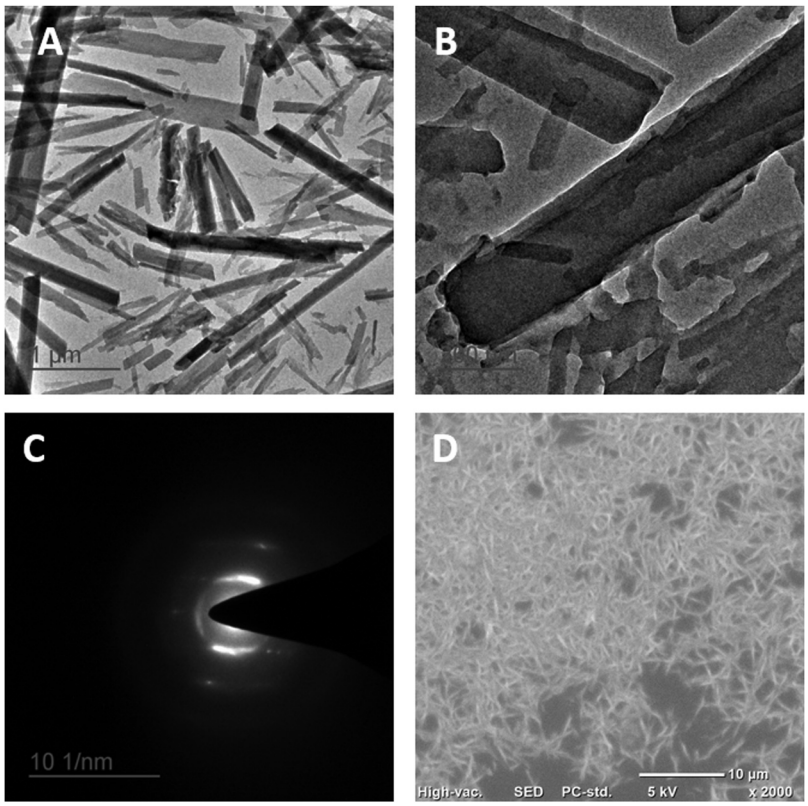

Fig. 2 (A) Low magnification TEM image of Qu–NCs (scale bar 1 µm); (B) high magnification TEM image of Qu–NCs (scale bar 1 µm); (C) SAED image of Qu–NCs (scale bar 1 µm); (D) SEM image of Qu–NCs (scale bar 10 µm).

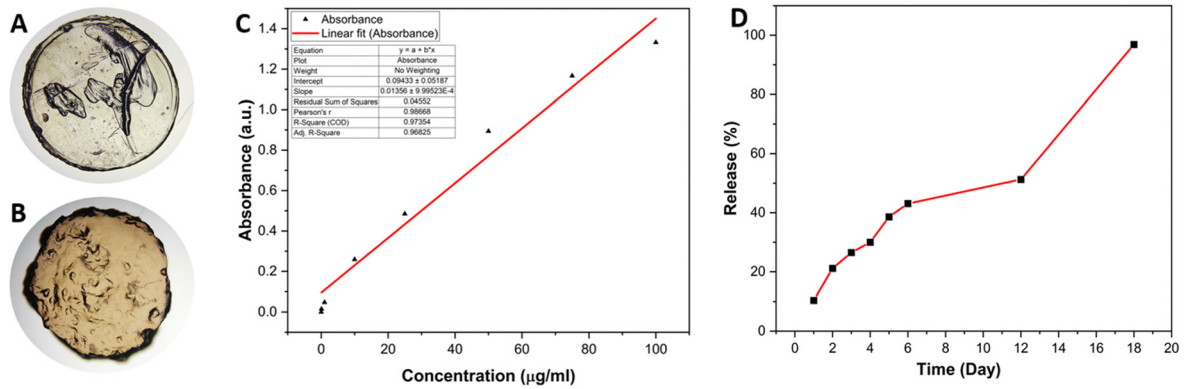

Fig. 3 (A) Brightfield microscopy image of alginate patch; (B) brightfield microscopy image of Qu–NC hydrogel; (C) standard curve of quercetin; (D) release (%) of quercetin from Qu–NC hydrogel.

profile exhibited a slow and steady pattern, with approximately 10.39%, 30.00%, and 43.10% of the quercetin released by day 1, day 4, and day 6, respectively. The slow and steady release pattern observed over 18 days suggests the potential for this system to provide prolonged therapeutic effects at the wound site. The initial burst release of approximately 10% by day 1 could be attributed to loosely bound quercetin molecules on the outer surface of the hydrogel.

Subsequently, the sustained release observed throughout the study indicates the controlled release of quercetin entrapped within the alginate matrix. This controlled release profile is advantageous for wound healing applications, as it allows for a continuous supply of quercetin to the wound site, potentially enhancing its therapeutic efficacy and reducing the frequency of dosing.[29,30] The rate of drug release from the hydrogel matrix became faster compared to that of free quercetin-containing hydrogel, which is important for the potent delivery of any poorly water-soluble compound (Fig. S1, ESI†). Wound beds are mainly wet and are rich in plasma proteins. Following the application of the Qu–NCs loaded hydrogel patch, a faster drug release occurs along with faster diffusion rates of the drug from hydrogel (Fig. S3, ESI†).

In addition, the presence of various proteins in the wound microenvironment causes a faster degradation rate of hydrogel, stimulating higher drug release and elevated drug amount in the wound locally to improve the therapeutic outcome.[31]

3.3 *In vitro* degradation studies

The degradation behaviour of the hydrogels was investigated by monitoring their weight changes over 12 days in phosphate-buffered saline (PBS). The quercetin nanocrystal (Qu–NC) loaded hydrogel exhibited a slower degradation profile compared to the blank hydrogel. The weight percentage of the Qu–NC hydrogel remained significantly higher at each time point: 78.10%, 72.27%, 42.63%, and 12.63% on days 3, 5, 7, and 12, respectively, compared to the blank hydrogel (85.90%, 45.70%, 28.00%, and 6.28%). This trend was further corroborated by microscopy images (Fig. 4A and B), which visually demonstrated less deformation in the Qu–NC hydrogel compared to the blank hydrogel over time.

The slower degradation rate of the Qu–NC hydrogel can be attributed due to the formation of inter-molecular hydrogen bonding of alginate with embedded nanocrystals within the alginate matrix, potentially leading to enhanced structural stability and prolonged drug release. The comparative bar plot (Fig. 4C) clearly visualizes the difference in weight percentage between the two hydrogel groups, supporting the findings of a slower degradation rate for the Qu–NC loaded hydrogel.

3.4 Mechanical and viscoelastic properties of the Qu–NC hydrogel

Analysis of the stress–strain data revealed superior performance of the Qu–NC hydrogel under both deformation levels (10% and 15%), indicating a significant improvement in its mechanical strength. The compression test revealed similar mechanical properties for both Qu–NC hydrogel and the blank hydrogel at 10% compression, exhibiting good elasticity with a compressive stress of approximately 0.015 N m^{-2} (Fig. 5A). While both hydrogels retained their elastic properties at 15% strain (Fig. 5B), the Qu–NC hydrogel displayed a slightly lower stress (around 0.021 N m^{-2}) compared to the blank hydrogel (0.023 N m^{-2}). The viscoelastic properties were further evaluated by performing amplitude and frequency sweep tests. The amplitude sweep was performed to determine the yield stress and deformation behaviour or linear viscoelastic range (LVR) in the non-destructive deformation range at a constant frequency of 1 rad s^{-1}. As shown in Fig. 5C, all hydrogels revealed predominant elastic behaviour at a low shear rate ($G' > G''$). A frequency sweep in the LVR region was also performed to describe the structure and viscoelastic nature of the hydrogels, as depicted in Fig. 5D. For the frequency sweep, a constant strain of 1% was applied and G' and G'' were plotted as a function of the frequency. As can be seen from Fig. 5D, all gels show $G' > G''$ over the given frequency range, indicating their predominantly elastic nature and stability over long-term storage due to a stable network of forces. In addition, both G' and G'' are nearly constant and independent across the entire frequency range from 0.1 to 10 rad s^{-1}. This suggests that the incorporation of quercetin nanocrystals reinforces the hydrogel structure, potentially enhancing yield strength, compressive strength, and breaking strength. Including these specific strength values and a visual representation of the stress–strain curves would further solidify these findings. Overall, the test demonstrates the promise of Qu–NC hydrogels as robust and resilient materials due to their superior mechanical properties under compression.

3.5 Biocompatibility assessment using the CAM assay, MTT assay and skin irritation assay

The chorioallantoic membrane (CAM) assay was employed to evaluate the biocompatibility of the quercetin nanocrystal (Qu–NC) loaded hydrogel with living tissue. Chick embryos were treated with the hydrogel patch, and blood vessel formation on the CAM was monitored over time. Visual inspection and image capture with a stereo microscope at different time points up to 12 hours post-treatment (Fig. 6A) revealed no apparent negative effects of the Qu–NC hydrogel on blood vessel formation or vascular network integrity.

To check the biological safety of the synthesized nanomaterial, we performed the *in vivo* skin irritation test in a rat model. The findings from the acute dermal irritation study of both the Qu–NC and positive control (5% formaldehyde) in rats are shown in Fig. 6B. No adverse dermal responses, including edema and erythema, were observed in the skin after applying

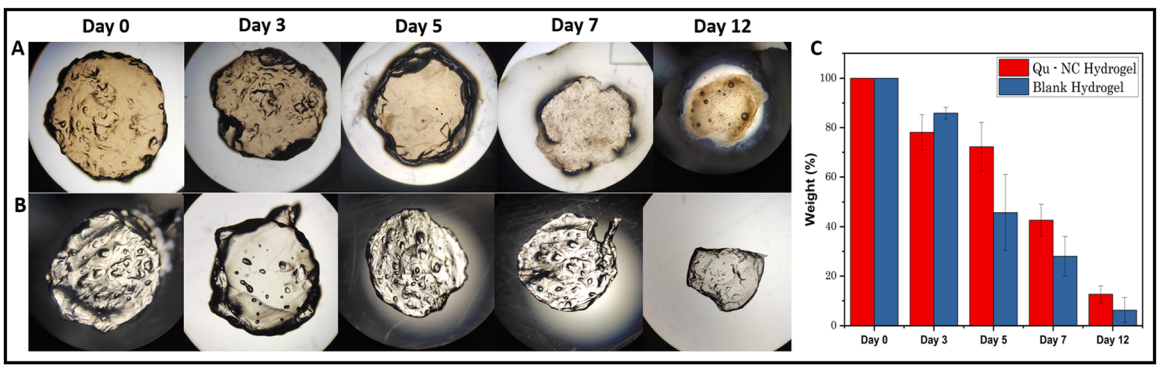

Fig. 4 (A) Degradation image of Qu–NC hydrogel and (B) blank hydrogel; (C) degradation plot of Qu–NC hydrogel and blank hydrogel.

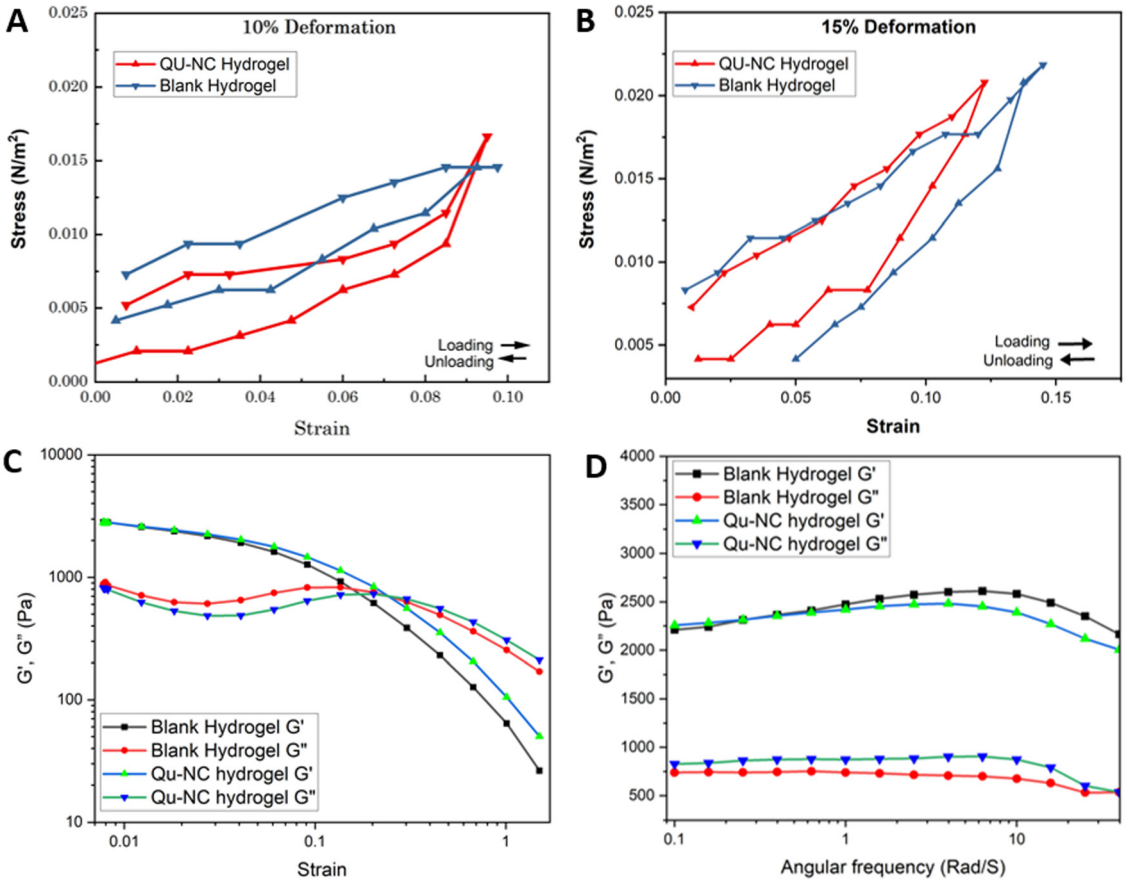

Fig. 5 (A) The compressive loading–unloading curves of blank hydrogel and Qu–NC hydrogel at 10% deformation. (B) The compressive loading–unloading curves of blank hydrogel and Qu–NC hydrogel at 15% deformation. (C) Amplitude sweep at a constant frequency of 1 rad s^{-1}. (D) Frequency sweep at a constant shear strain of 1%.

1 mg mL^{-1} Qu–NC solution to the skin. On the other hand, the standard skin irritant (5% formaldehyde) group showed severe erythema and edema after 72 hours of topical application. The results confirm that Qu–NC can be used for dermal application as it is non-irritant and compatible with the skin. To evaluate the biocompatibility of the hydrogels, HEK-293T cells were cultured in the presence of Qu–NC hydrogel and blank hydrogel for 24 hours. Cell viability was assessed using the MTT assay, which measures the metabolic activity of cells. The results, depicted in Fig. 6C, demonstrate that both the Qu–NC hydrogel and the blank hydrogel exhibited excellent biocompatibility, with cell viability exceeding 90% for the Qu–NC hydrogel and 99% for the blank hydrogel. These findings suggest that the hydrogels are well-tolerated by cells and have potential for biomedical applications, including drug delivery and wound healing.

3.6 Qu–NC shows dose-dependent antioxidant properties and *in vitro* ROS clearance

The free radical scavenging potential of the quercetin nanocrystal (Qu–NC), Qu–NC hydrogel, and free quercetin was evaluated using a DPPH assay.[32] The Qu–NC exhibited dose-dependent free radical scavenging activity (Fig. 7A). As the concentration of Qu–NC increased (25–84 mg mL^{-1}), the percentage of radical scavenging activity (RSA%) proportionally increased from 50% to 83%. This concentration-dependent response suggests the ability of Qu–NC to efficiently scavenge free radicals, potentially contributing to its therapeutic effects.

The DPPH assay further revealed that the Qu–NC hydrogel retained its antioxidant properties even after encapsulation (Fig. 7B). The hydrogel demonstrated a stable RSA% of approximately 55–60% across all tested concentrations, indicating the successful incorporation of quercetin and its sustained release from the hydrogel matrix. The *in vitro* ROS clearance assay in *E. coli* has been done by using 2′-7′-dichlorodihydrofluorescein diacetate (DCFH-DA). In the presence of ROS, DCFH is oxidized to form highly fluorescent DCF (2′,7′-dichlorofluorescein), generating green fluorescence.[33] The results show that Qu–NC hydrogel-treated bacteria show less fluorescence intensity (2881.65 ± 475) compared to that of the untreated control group (6190 ± 1303). The results indicate that Qu–NC hydrogel treatment can be utilized to eliminate intra-cellular ROS effectively (Fig. 7C).

The observed dose-dependent free radical scavenging activity of the Qu–NC complex aligns with previous reports attributing the antioxidant properties of quercetin to its ability to directly scavenge free radicals and enhance the body's endogenous

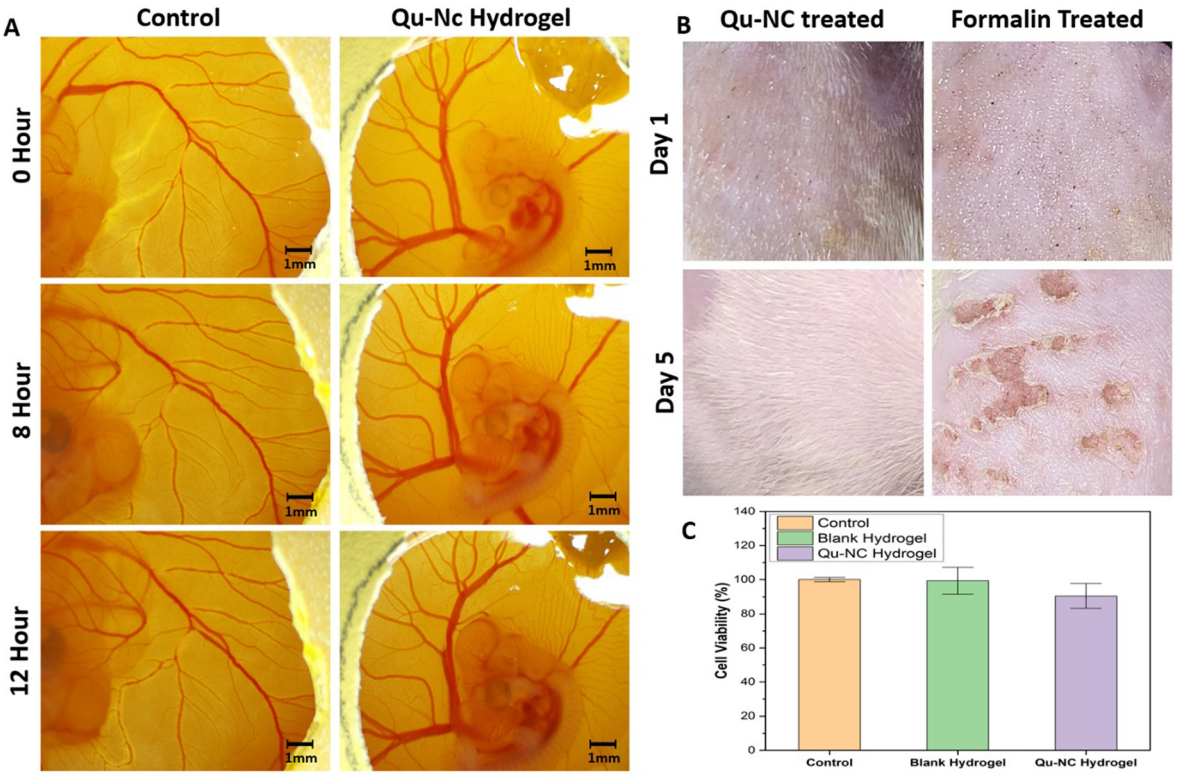

Fig. 6 (A) Microscopy images of chick embryo chorioallantoic membrane at 0 hour, 8 hours and 12 hours of control and Qu–NC hydrogel treated groups. (B) The photograph of the skin irritation study shows no irritation in the Qu–NC treated group compared to the formalin treated group. (C) The cell viability plot of blank hydrogel and Qu–NC hydrogel shows good biocompatibility ($P > 0.05$).

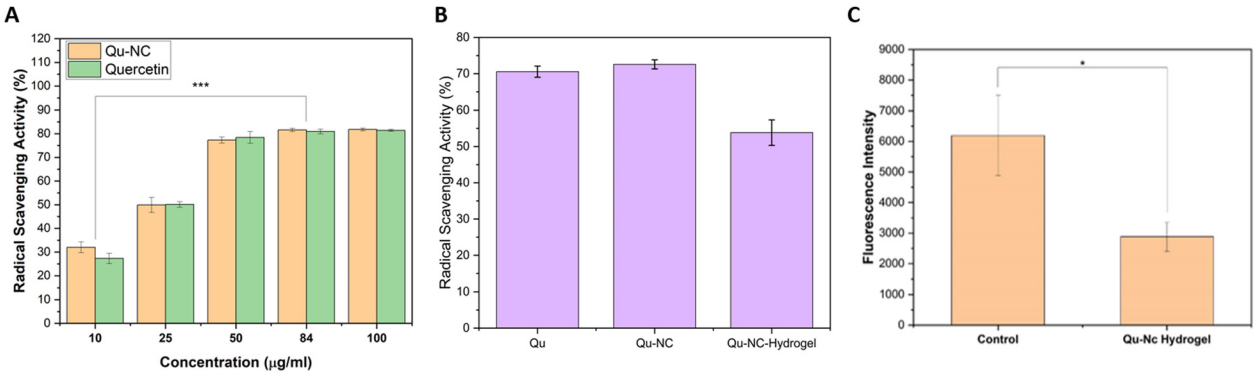

Fig. 7 Anti-oxidant properties of Qu–NCs and Qu–NC loaded hydrogel. (A) Dose dependent radical scavenging activity of Qu–NCs. (B) Radical scavenging activity of Qu–NC loaded hydrogel compared with quercetin drug and nanocrystals ($P > 0.05$). (C) In cell ROS production assay in *E. coli* upon treatment with Qu–NC loaded hydrogel ($P < 0.05$).

antioxidant defence systems.[34] This antioxidant activity is crucial in wound healing, as excessive free radicals can contribute to tissue damage and hinder the healing process.[35] By effectively scavenging free radicals, Qu–NCs have the potential to promote a favourable wound-healing environment by minimizing oxidative stress and promoting tissue repair.[36]

3.7 *In vivo* wound healing assessment

The *in vivo* wound healing efficacy of the quercetin nanocrystal (Qu–NC) loaded hydrogel was assessed in a full-thickness excision wound model on the dorsal side of Wistar rats. Fig. 8A depicts the graphical representation of the treatment timeline. Visual observation and digital image analysis (Fig. 8C) revealed a significantly faster rate of wound closure in the Qu–NC hydrogel group compared to the blank hydrogel and control groups. Quantitative wound closure data (Fig. 8B) confirmed this observation, with the Qu–NC hydrogel group achieving nearly complete wound closure (90.45%) by day 10, while the blank hydrogel and control groups exhibited lower closure rates (79.41% and 69.50%, respectively). This enhanced

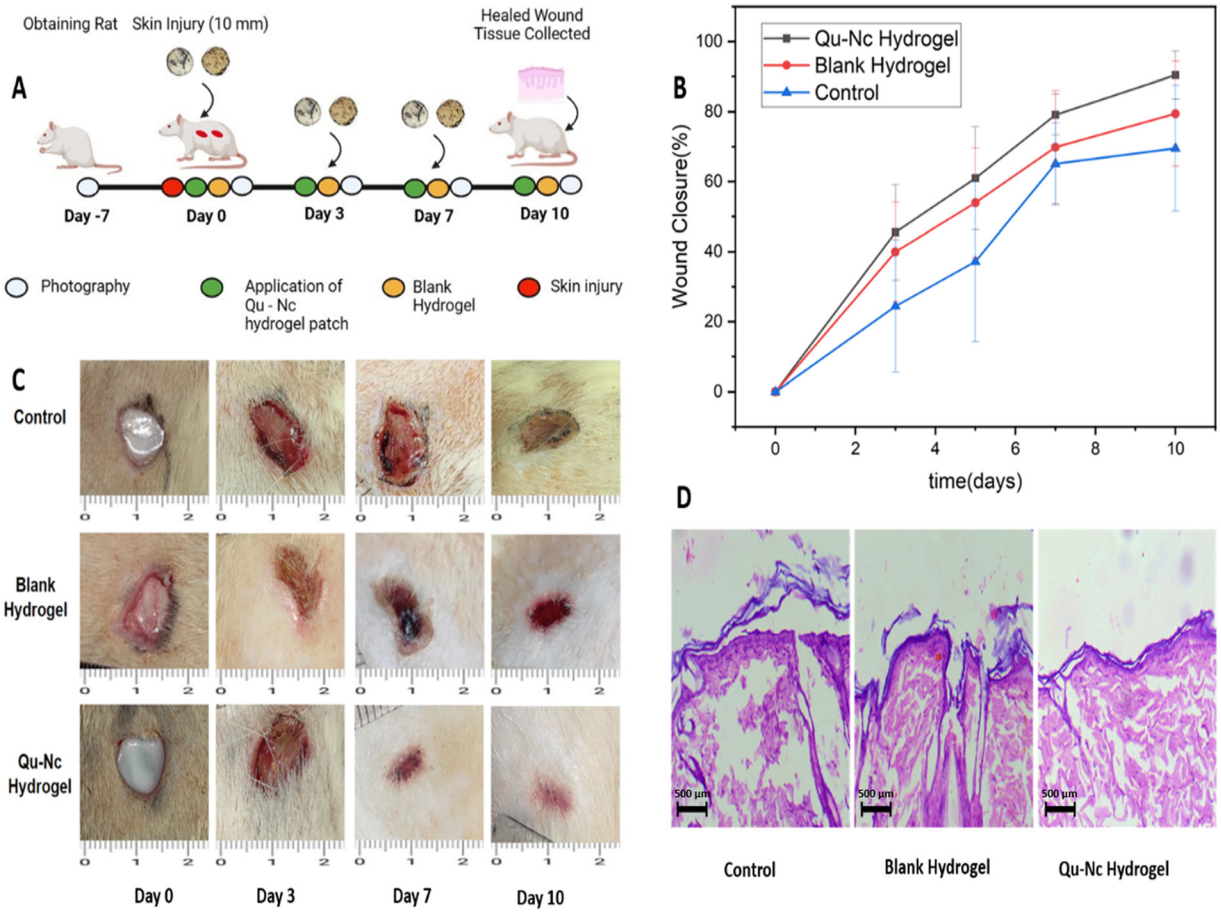

Fig. 8 (A) Schematic representation of the establishment and wound treatment in Wistar rats, (B) the wound closure curve of wound area for the treated and untreated groups, (C) the optical photographs of wounds from day 0 to day 10 for the Qu–NC hydrogel treated, blank hydrogel treated and control groups, and (D) the microscopic HE staining of rat skin wounds after 10 days for the control, blank hydrogel and Qu–NC hydrogel treated groups. Images were taken at 20× magnification.

wound healing efficacy observed with Qu–NC hydrogel treatment suggests its potential for promoting faster and more efficient healing processes.

Histological analysis using HE staining (Fig. 8D) further supported the wound-healing efficacy of the Qu–NC hydrogel. The Qu–NC hydrogel group displayed proper epithelialization with a well-developed and intact epidermal layer at day 10. In contrast, the blank hydrogel and control groups exhibited a less developed epidermal layer with signs of damage. Additionally, the Qu–NC hydrogel group showed minimal inflammation compared to the other groups, and no signs of necrosis were observed in any group, indicating good biocompatibility. Notably, treatment with Qu–NC hydrogel also promoted fibrosis-free recovery, suggesting minimal scar formation and preservation of the integrity of the local skin tissue. A collagen immunohistochemistry staining assay supported the uniform collagen deposition in the wound bed in the Qu–NC hydrogel-treated group. As shown in Fig. 9E and F, a good amount of collagen deposition and regular distribution of collagen was observed in the Qu–NC hydrogel-treated group. On the other hand, the control and blank hydrogel group shows irregular amounts of collagen deposition in the skin tissue. Considering these assays, it can be confirmed that hydrogel-loaded quercetin is highly efficient in complete and rapid wound healing.

α-SMA staining is used to determine the expression of myofibroblasts, prominent during the regeneration phase of wound healing in the dermis and subcutis. Moreover, α-SMA can also be utilized to analyse endothelial cells of new blood vessels. Fig. 9A and B represent the α-SMA staining of the tissues, where the proportion of positive α-SMA intensity was higher (∼1.66 times) in Qu–NC hydrogel-treated groups compared to the untreated control on day 12 (Fig. 9G). CD163 is a marker of M2 macrophages, which possess anti-inflammatory properties. Immunohistochemical staining revealed significantly higher expression of CD163 in the Qu–NC hydrogel treated group in comparison with the control group (Fig. 9C and D). Quantitative analysis using ImageJ confirmed a nearly 1.5-fold increase in CD163-positive cells in the Qu–NC hydrogel treated group compared to the untreated control group (Fig. 9H). These findings suggest that AgSCN-NPs promote a more favourable wound healing environment by inducing a shift towards an anti-inflammatory M2 macrophage phenotype.

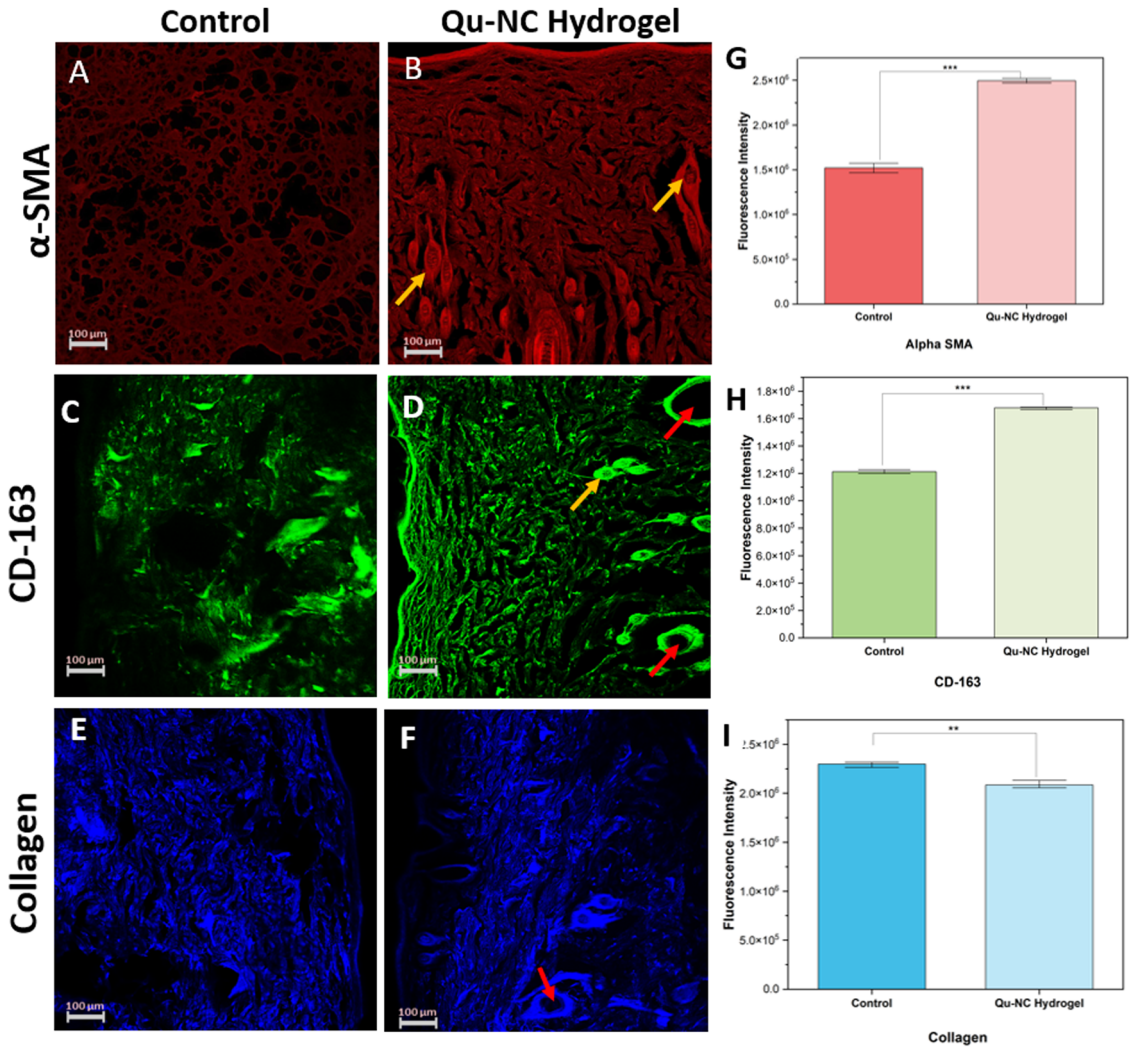

Fig. 9 (A) and (B) Confocal microscopic images of alpha SMA immunostaining in control and Qu–NC hydrogel treated rat skin after 10 days; (C) and (D) confocal microscopic images of CD163 immunostaining in control and Qu–NC hydrogel treated rat skin after 10 days; (E) and (F) confocal microscopic images of collagen immunostaining in control and Qu–NC hydrogel treated rat skin after 10 days (red arrow represents the blood vessel and yellow arrow represents the hair follicles in the treated sample). (G)–(I) Quantification plot of overall fluorescence intensity of alpha SMA positive cells, CD163 positive cells and collagen positive cells; respectively.

3.8 *In vivo* antioxidant assessment through a diabetic wound model

Diabetic mice exhibit elevated levels of reactive oxygen species (ROS) due to hyperglycemia-induced oxidative stress.[37] We induced diabetes in BALB/c mice by intraperitoneal injection of streptozotocin (50 mg kg^{-1} body weight). Two days later, full-thickness wounds were created on the backs of these mice (Fig. 10A). Treatment with Qu–NC hydrogel (applied topically on days 1, 3, 5, and 7) significantly accelerated wound closure compared to the control group. After 9 days, the Qu–NC hydrogel-treated group exhibited 93.69 ± 2.547% wound closure, while the control group showed only 52 ± 20.24% closure (Fig. 10B and C).

To further corroborate the antioxidant properties of Qu–NC hydrogel, we assessed lipid peroxidation and reduced glutathione (GSH) levels in wound tissues. We observed a significant decrease in malondialdehyde (MDA), a marker of lipid peroxidation, in the Qu–NC hydrogel-treated group compared to the control group. The Qu–NC hydrogel-treated group exhibited an MDA level of 34.76 nmol mg^{-1} protein, significantly lower than the control group's 70.36 nmol mg^{-1} protein (Fig. 10D). Conversely, the GSH level, a key antioxidant, which has an essential role in many intracellular functions, including reductive processes for proteins and DNA synthesis, was significantly increased in the treated group. The Qu–NC hydrogel-treated group showed a GSH level of 0.547 U mg^{-1} protein, while the control group had a level of 0.424 U mg^{-1} protein (Fig. 10E).

These findings strongly suggest that Qu–NC hydrogel possesses potent antioxidant properties that contribute to its efficacy in promoting wound healing in an oxidative stress model. Our results provide compelling evidence for the

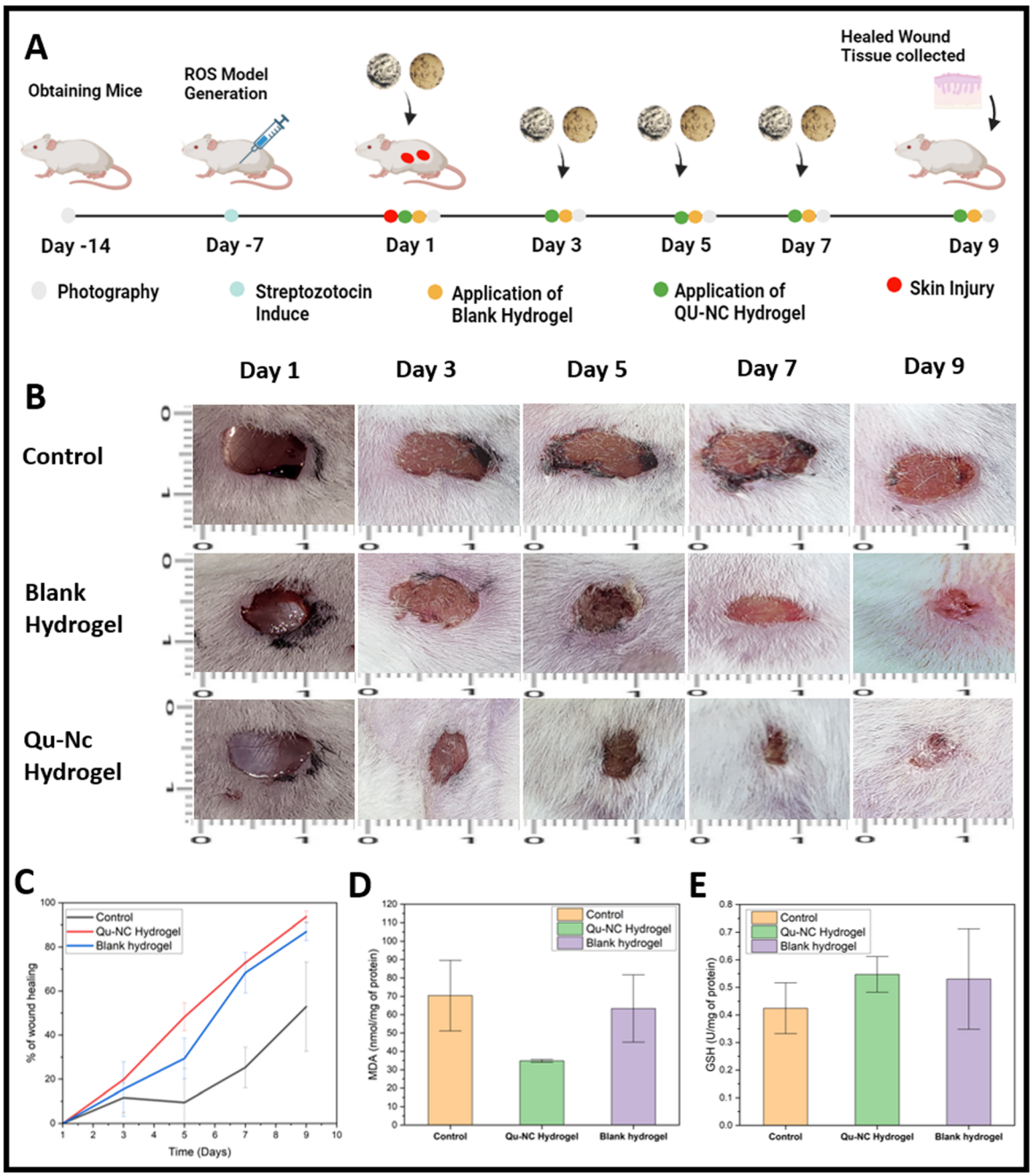

Fig. 10 (A) Schematic representation of the establishment of an ROS model and wound treatment in BALB/c mice. (B) The optical photographs of wounds from day 1 to day 9 for the Qu–NC hydrogel treated, blank hydrogel treated and control groups. (C) The wound closure curve of wound area for each group (n = 3) ($P > 0.05$). (D) Estimation of MDA content in each treatment group compared with control ($P > 0.05$). (E) Estimation of GSH content in each treatment group compared with control ($P > 0.05$).

therapeutic potential of this novel hydrogel in various oxidative stress-related conditions.

The *in vivo* wound healing results demonstrate the effectiveness of the Qu–NC loaded hydrogel in accelerating wound closure compared to the blank hydrogel and control groups. This enhanced efficacy can be attributed to several factors. The sustained release of quercetin from the hydrogel likely plays a crucial role. Quercetin possesses anti-inflammatory[38] and antioxidant properties that can promote tissue regeneration and reduce oxidative stress, both of which are essential for efficient wound healing. Additionally, the nanocrystals within the hydrogel matrix might contribute to its wound-healing potential by providing a scaffold for cell migration and promoting tissue repair. The histological analysis further strengthens these findings, revealing improved re-epithelialization, reduced inflammation, higher uniform collagen deposition, new blood vessel formation, fibroblast growth and minimal scar formation in the Qu–NC hydrogel group. Overall, these results highlight the

promising potential of Qu–NC-loaded alginate hydrogels as a novel and effective wound-healing therapy.

While quercetin's potential for wound healing has been explored,[10–12,39] our study offers distinct advantages. The core innovation of this work lies in the development of a quercetin nanocrystal-loaded hydrogel to stimulate rapid drug release, sustained drug release for over 2 weeks, better stability and improved solubility of the quercetin. By improving the physicochemical properties of the drug, an improved therapeutic window (with faster wound healing time) and efficiency were achieved compared to the existing published literature (Table 1). It is important to highlight that Qu–NC hydrogel was able to heal the regular wounds within 10 days in a rat model of skin wounds. In contrast, chronic diabetic wounds in a mouse model were healed within 9 days of Qu–NC hydrogel treatment. This confirms the rapid healing efficiency of Qu–NC hydrogel in regular and chronic wound models. Moreover, the hydrogel system enables controlled and sustained release of the drug for 18 days, addressing the limitations associated with conventional topical formulations. This novel approach not only improves drug bioavailability but also provides a more effective therapeutic strategy for wound healing by ensuring a consistent drug concentration at the wound site. The incorporation of quercetin nanocrystals (Qu–NCs) within an alginate hydrogel provides a controlled and sustained release mechanism, with increased solubility overcoming limitations associated with rapid degradation and low bioavailability often seen in traditional topical quercetin delivery. Additionally, the Qu–NCs themselves exhibit potent antioxidant activity, a crucial aspect for promoting wound healing by reducing oxidative stress. This advantage may not be explicitly addressed in all existing quercetin-based wound dressings. Furthermore, our Qu–NC hydrogel offers a multifaceted therapeutic approach. The sustained release of quercetin provides anti-inflammatory and antioxidant benefits, while the hydrogel matrix itself might facilitate cell migration and tissue repair. This combination has the potential to yield superior results compared to single-agent therapies.

However, our study also has limitations. The *in vivo* evaluation utilized rodent models, and further investigations in larger animal models with a closer resemblance to human skin physiology are necessary for a more comprehensive assessment. Additionally, while our work suggests potential mechanisms, a more detailed understanding of the precise molecular pathways by which the Qu–NC hydrogel promotes wound healing is required. Future research will address these limitations.

4. Conclusion

This study presented the development and evaluation of a novel quercetin nanocrystal (Qu–NC) loaded alginate hydrogel for wound healing applications. The successful fabrication of the hydrogel with controlled drug-release properties was demonstrated. The Qu–NC complex exhibited potent antioxidant activity, suggesting its potential to combat oxidative stress and promote a favourable healing environment. Furthermore, *in vitro* studies revealed the sustained release of quercetin from the hydrogel matrix. *In vivo* wound healing studies using a rat model confirmed the efficacy of the Qu–NC hydrogel. Compared to the blank hydrogel and control groups, the Qu–NC hydrogel group exhibited significantly faster wound closure rates in both a rat model and diabetic mouse model. Histological analysis further supported these findings, demonstrating improved re-epithelialization, reduced inflammation, and minimal scar formation in the Qu–NC hydrogel-treated wounds. Quercetin nanocrystal-loaded alginate hydrogels hold immense promise for promoting efficient wound closure, reducing healing time, and improving patient outcomes.

Table 1 Table of comparison between previously published studies and this study

Dosage	Wound size	Time	% wound closure	Highlights of the paper	Ref.
6%	10 mm	Day 10	90.4 ± 6.8%	• This study uses minimum dosage and shows effective wound healing in 10 days with an average wound size of 10 mm. • Mechanically stable hydrogel. • Antioxidant property. • 68.31% Drug release in 24 h.	This article
0.00151%	9 mm	Days 18	98.42%	• To increase the solubility, they used Tween 80, Labrasol, Labrafac, Transcutol Hp, polyvinylpyrrolidone and PEG 400. • Used silver nanoparticles and quercetin with hydrogel • 75–80% drug release from quercetin silver nanoparticles in 12 h.	40
0.03%	4 mm	Days 8	94.75%	• Treatment directed no sustained delivery of drug and no mechanical strength. • Dimension of wound is very small. • No solubility assay	10
0.1%	20 mm	Days 11	70%	• Topically applied shows no mechanical stability and sustained release. • Nanocrystals were not formed. • No solubility assay	12
0.5%	10 mm	Days 16	98%	• Liposome loaded quercetin incorporated in hydrogel. • The hydrogel assisted in maintaining the humectant property of skin. • 68.31% drug release in 24 h.	41
0.075%	20 mm	Days 14	100%	• Quercetin loaded alginate chitosan nanoparticles used. • No interference with adsorption of nutrients. • Quercetin alginate chitosan gel shows 62.51% release in 24 h.	42

Author contributions

M. N. and S. M. designed the studies and formulated the project. M. N., V. K., D. B., L. P., and P. K. performed all the experiments. The manuscript was written by M. N., V. K. and S. M. S. M. supervised the project and acquired the funding for the work. All authors have approved the final version of the manuscript.

Data availability

All the data of this article are available on the following link **https://www.scidb.cn/en/anonymous/aVFOM3Vh**.

Conflicts of interest

There are no conflicts to declare.

Acknowledgements

SM acknowledges DBT, India (BT/PR49530/MED/32/839/2023) for providing funding support. We also acknowledge the central instrument facility (CIF), IIT (BHU) and director of the Indian Institute of Technology (BHU), Varanasi, India, for continuous support. MN is grateful to MHRD, and LP and DB are grateful to UGC for their fellowship support.

References

1 S. Enoch and D. J. Leaper, *Surgery*, 2008, **26**, 31–37.
2 R. S. Kirsner and W. H. Eaglstein, *Dermatol. Clin.*, 1993, **11**, 629–640.
3 A. C. d O. Gonzalez, T. F. Costa, Z. d A. Andrade and A. R. A. P. Medrado, *An. Bras. Dermatol.*, 2016, **91**, 614–620.
4 M. Flanagan, *J. Wound Care*, 2000, **9**, 299–300.
5 G. S. Kelly, *Altern. Med. Rev.*, 2011, **16**, 172–195.
6 Y.-Z. Zheng, G. Deng, Q. Liang, D.-F. Chen, R. Guo and R.-C. Lai, *Sci. Rep.*, 2017, **7**, 7543.
7 C. Tian, X. Liu, Y. Chang, R. Wang, T. Lv, C. Cui and M. Liu, *S. Afr. J. Bot.*, 2021, **137**, 257–264.
8 L. W. Nitiema, A. Savadogo, J. Simpore, D. Dianou and A. S. Traore, *Int. J. Microbiol. Res.*, 2012, **3**, 183–187.
9 X. Cai, Z. Fang, J. Dou, A. Yu and G. Zhai, *Curr. Med. Chem.*, 2013, **20**, 2572–2582.
10 Y. Mi, L. Zhong, S. Lu, P. Hu, Y. Pan, X. Ma, B. Yan, Z. Wei and G. Yang, *J. Ethnopharmacol.*, 2022, **290**, 115066.
11 K. M. Doersch and M. K. Newell-Rogers, *Exp. Biol. Med.*, 2017, **242**, 1424–1431.
12 V. Kant, B. L. Jangir, V. Kumar, A. Nigam and V. Sharma, *Growth Factors*, 2020, **38**, 105–119.
13 D. Yenurkar, M. Nayak and S. Mukherjee, *Nanoscale Adv.*, 2023, **5**, 4018–4040.
14 A. J. Smith, P. Kavuru, L. Wojtas, M. J. Zaworotko and R. D. Shytle, *Mol. Pharmaceutics*, 2011, **8**, 1867–1876.
15 J. A. Hubbell, *J. Controlled Release*, 1996, **39**, 305–313.
16 R. Pereira, A. Carvalho, D. C. Vaz, M. Gil, A. Mendes and P. Bártolo, *Int. J. Biol. Macromol.*, 2013, **52**, 221–230.
17 Q. Zeng, Y. Han, H. Li and J. Chang, *J. Mater. Chem. B*, 2015, **3**, 8856–8864.
18 Y. Han, Y. Li, Q. Zeng, H. Li, J. Peng, Y. Xu and J. Chang, *J. Mater. Chem. B*, 2017, **5**, 3315–3326.
19 N. Xu, Y. Yuan, L. Ding, J. Li, J. Jia, Z. Li, D. He and Y. Yu, *Int. J. Burns Trauma*, 2022, **10**, tkac019.
20 L. Pradhan, P. Sah, M. Nayak, A. Upadhyay, P. Pragya, S. Tripathi, G. Singh, B. Mounika, P. Paik and S. Mukherjee, *JBIC, J. Biol. Inorg. Chem.*, 2024, 1–21.
21 M. Nayak, L. Sonowal, L. Pradhan, A. Upadhyay, P. Kamath and S. Mukherjee, *Chem. – Asian J.*, 2024, e202400187.
22 J. K. Chan, *Int. J. Surg. Pathol.*, 2014, **22**, 12–32.
23 D. He, X. Liu, J. Jia, B. Peng, N. Xu, Q. Zhang, S. Wang, L. Li, M. Liu, Y. Huang, X. Zhang, Y. Yu and G. Luo, *Adv. Funct. Mater.*, 2024, **34**, 2306357.
24 A. Kumari, S. K. Yadav, Y. B. Pakade, B. Singh and S. C. Yadav, *Colloids Surf., B*, 2010, **80**, 184–192.
25 M. Kokalj Ladan, J. Straus, E. Tavčar Benković and S. Kreft, *Sci. Rep.*, 2017, **7**, 7226.
26 S. N. Abd El-Rahmanand and S. Suhailah, *Indian J. Drugs*, 2014, **2**, 96–103.
27 J. L. Lábár, *Microsc. Microanal.*, 2008, **14**, 287–295.
28 X. Zhang, H. Xing, Y. Zhao and Z. Ma, *Pharmaceutics*, 2018, **10**, 74.
29 A. Stockwell, S. Davis and S. Walker, *J. Controlled Release*, 1986, **3**, 167–175.
30 A. Badwan, A. Abumalooh, E. Sallam, A. Abukalaf and O. Jawan, *Drug Dev. Ind. Pharm.*, 1985, **11**, 239–256.
31 R. Zhang, Y. Tian, L. Pang, T. Xu, B. Yu, H. Cong and Y. Shen, *ACS Appl. Mater. Interfaces*, 2022, **14**, 10187–10199.
32 A. A. Mandal, A. Upadhyay, A. Mandal, M. Nayak, M. S. K, S. Mukherjee and S. Banerjee, *ACS Appl. Mater. Interfaces*, 2024, **16**(22), 28118–28133.
33 A. Aranda, L. Sequedo, L. Tolosa, G. Quintas, E. Burello, J. Castell and L. Gombau, *Toxicol. In Vitro*, 2013, **27**, 954–963.
34 A. W. Boots, G. R. Haenen and A. Bast, *Eur. J. Pharmacol.*, 2008, **585**, 325–337.
35 M. Liu, R. Ding, Z. Li, N. Xu, Y. Gong, Y. Huang, J. Jia, H. Du, Y. Yu and G. Luo, *Adv. Sci.*, 2024, **11**, 2306602.
36 C. K. Sen, S. Khanna, G. Gordillo, D. Bagchi, M. Bagchi and S. Roy, *Ann. N. Y. Acad. Sci.*, 2002, **957**, 239–249.
37 N. Xu, Y. Gao, Z. Li, Y. Chen, M. Liu, J. Jia, R. Zeng, G. Luo, J. Li and Y. Yu, *Chem. Eng. J.*, 2023, **466**, 143173.
38 A. W. Boots, L. C. Wilms, E. L. Swennen, J. C. Kleinjans, A. Bast and G. R. Haenen, *Nutrition*, 2008, **24**, 703–710.
39 G. Yin, Z. Wang, Z. Wang and X. Wang, *Exp. Dermatol.*, 2018, **27**, 779–786.
40 R. Badhwar, B. Mangla, Y. R. Neupane, K. Khanna and H. Popli, *Nanotechnology*, 2021, **32**, 505102.
41 R. Jangde, S. Srivastava, M. R. Singh and D. Singh, *Int. J. Biol. Macromol.*, 2018, **115**, 1211–1217.
42 T. Nalini, S. Khaleel Basha, A. Mohamed Sadiq and V. Sugantha Kumari, *Polym. Bull.*, 2023, **80**, 515–540.